Vessel Tracking via Sub-Riemannian Geodesics on the Projective Line Bundle

E.J. Bekkers[1*], R. Duits[1*], A. Mashtakov[2*], and Yu. Sachkov[2⋆]

[1] Eindhoven University of Technology, The Netherlands,
Department of Mathematics and Computer Science,
[2] Program Systems Institute of RAS, Russia,
Control Processes Research Center
{E.J.Bekkers, R.Duits}@tue.nl, {alexey.mashtakov, yusachkov}@gmail.com

Abstract. We study a data-driven sub-Riemannian (SR) curve optimization model for connecting local orientations in orientation lifts of images. Our model lives on the projective line bundle $\mathbb{R}^2 \times P^1$, with $P^1 = S^1/_\sim$ with identification of antipodal points. It extends previous cortical models for contour perception on $\mathbb{R}^2 \times P^1$ to the data-driven case. We provide a complete (mainly numerical) analysis of the dynamics of the 1st Maxwell-set with growing radii of SR-spheres, revealing the cut-locus. Furthermore, a comparison of the cusp-surface in $\mathbb{R}^2 \times P^1$ to its counterpart in $\mathbb{R}^2 \times S^1$ of a previous model, reveals a general and strong reduction of cusps in spatial projections of geodesics. Numerical solutions of the model are obtained by a single wavefront propagation method relying on a simple extension of existing anisotropic fast-marching or iterative morphological scale space methods. Experiments show that the projective line bundle structure greatly reduces the presence of cusps. Another advantage of including $\mathbb{R}^2 \times P^1$ instead of $\mathbb{R}^2 \times S^1$ in the wavefront propagation is reduction of computational time.

Keywords: Sub-Riemannian geodesic, tracking, projective line bundle

1 Introduction

In image analysis extraction of salient curves such as blood vessels, is often tackled by first lifting the image data to a new representation defined on the higher dimensional space of positions and directions, followed by a geodesic tracking [1–3] in this lifted space [4–6]. Benefits of such approaches are that one can generically deal with complex structures such as crossings [4, 6, 7], bifurcations [8], and low-contrast [5, 6, 9], while accounting for contextual alignment

⋆ Joint main authors. The ERC is gratefully acknowledged for financial support (ERC-StG nr. 335555). Sections 1, 2 of the paper are written by R. Duits and A. Mashtakov, Section 3 is written by A. Mashtakov, Yu. Sachkov and R. Duits, Sections 4, 6 are written by R. Duits and A. Mashtakov, and Section 5 is written by E.J. Bekkers. The work of A. Mashtakov and Yu. Sachkov is supported by the Russian Science Foundation under grant 17-11-01387 and performed in Ailamazyan Program Systems Institute of Russian Academy of Sciences.

of local orientations [5, 6]. The latter can be done in the same way as in cortical models of visual perception of lines [10–13], namely via sub-Riemannian (SR) geometry on the combined space of positions and orientations. In these cortical models, it is sometimes stressed [12] that one should work in a projective line bundle $\mathbb{R}^2 \times P^1$ with a partition of equivalence classes $P^1 := S^1/_\sim$ with $\mathbf{n}_1 \sim \mathbf{n}_2 \Leftrightarrow \mathbf{n}_1 = \pm\mathbf{n}_2$. Furthermore, in the statistics of line co-occurrences in retinal images the same projective line bundle structure is crucial [14]. Also, for many image analysis applications the orientation of an elongated structure is a well defined characteristic of a salient curve in an image, in contrast to an artificially imposed direction.

At first sight the effect of the identification of antipodal points might seem minor as the minimizing SR geodesic between two elements in $\mathbb{R}^2 \times P^1$ is obtained by the minimum of the two minimizing SR geodesics in $\mathbb{R}^2 \times S^1$ that arise (twice) by flipping the directions of the boundary conditions. However, this appearance is deceptive, it has a rather serious impact on geometric notions such as 1) the 1st Maxwell set (where two distinct geodesics with equal length meet for the first positive time), 2) the cut-locus (where a geodesic looses optimality), 3) the cusp-surface (where spatial projections of SR geodesics show a cusp). Besides an analysis of the geometric consequences in Sect. 2, 3, 4, we show that the projective line bundle provides a better tracking with much less cusps in Sect. 5.

2 The Projective Line Bundle Model

The projective line bundle $\mathrm{PT}(\mathbb{R}^2)$ is a quotient of Lie group $\mathrm{SE}(2)$, and one can define a sub-Riemannian structure (SR) on it. The group $\mathrm{SE}(2) = \mathbb{R}^2 \rtimes SO(2)$ of planar roto-translations is identified with the coupled space of positions and orientations $\mathbb{R}^2 \times S^1$, and for each $g = (x, y, \theta) \in \mathbb{R}^2 \times S^1 \cong \mathrm{SE}(2)$ one has

$$L_g g' = g \odot g' = (x' \cos\theta + y' \sin\theta + x, -x' \sin\theta + y' \cos\theta + y, \theta' + \theta). \tag{1}$$

Via the push-forward $(L_g)_*$ one gets the left-invariant frame $\{\mathcal{A}_1, \mathcal{A}_2, \mathcal{A}_3\}$ from the Lie-algebra basis $\{A_1, A_2, A_3\} = \{\partial_x|_e\,, \partial_\theta|_e\,, \partial_y|_e\}$ at the unity $e = (0, 0, 0)$:

$$\mathcal{A}_1 = \cos\theta\,\partial_x + \sin\theta\,\partial_y, \quad \mathcal{A}_2 = \partial_\theta, \quad \mathcal{A}_3 = -\sin\theta\,\partial_x + \cos\theta\,\partial_y.$$

Let $\mathcal{C} : \mathrm{SE}(2) \to \mathbb{R}^+$ denote a smooth cost function strictly bounded from below. The SR-problem on $\mathrm{SE}(2)$ is to find a Lipschizian curve $\gamma : [0, T] \to \mathrm{SE}(2)$, s.t.

$$\begin{gathered} \dot\gamma(t) = u^1(t)\,\mathcal{A}_1|_{\gamma(t)} + u^2(t)\,\mathcal{A}_2|_{\gamma(t)}, \qquad \gamma(0) = g_0, \quad \gamma(T) = g_1, \\ l(\gamma(\cdot)) := \int_0^T \mathcal{C}(\gamma(t))\sqrt{\xi^2|u^1(t)|^2 + |u^2(t)|^2}\,\mathrm{d}t \to \min, \end{gathered} \tag{2}$$

with controls $u^1, u^2 : [0, T] \to \mathbb{R}$ are in $L^\infty[0, T]$, boundary points g_0, g_1 are given, $\xi > 0$ is constant, and terminal time $T > 0$ is free.

Thanks to reparametrization invariance the SR distance can be defined as

$$d(g_0,g_1) = \min_{\substack{\gamma\in \mathrm{Lip}([0,1],\mathrm{SE}(2)),\\ \dot\gamma\in\, \Delta|_\gamma\,,\ \gamma(0)=g_0,\gamma(1)=g_1}} \int_0^1 \sqrt{\mathcal{G}_{\gamma(\tau)}(\dot\gamma(\tau),\dot\gamma(\tau))}\,\mathrm{d}\tau, \tag{3}$$

with $\mathcal{G}_{\gamma(\tau)}(\dot\gamma(\tau),\dot\gamma(\tau)) = \mathcal{C}^2(\gamma(\tau))\left(\xi^2|u^1(\tau T)|^2+|u^2(\tau T)|^2\right)$, $\tau=\frac{t}{T}\in[0,1]$, and $\Delta := \mathrm{span}\{\mathcal{A}_1,\mathcal{A}_2\}$ with dual $\Delta^* = \mathrm{span}\{\cos\theta\,\mathrm{d}x+\sin\theta\,\mathrm{d}y,\mathrm{d}\theta\}$. The projective line bundle $\mathrm{PT}(\mathbb{R}^2)$ is a quotient $\mathrm{PT}(\mathbb{R}^2)=\mathrm{SE}(2)/_\sim$ with identification $(x,y,\theta)\sim(x,y,\theta+\pi)$. The SR distance in $\mathrm{PT}(\mathbb{R}^2)\cong\mathbb{R}^2\times P^1=\mathbb{R}^2\times\mathbb{R}/\{\pi\mathbb{Z}\}$ is

$$\begin{aligned}\overline{d}(q_0,\,q_1) &:= \min\{d(g_0,\,g_1)\,,\,d(g_0\odot(0,0,\pi),\,g_1\odot(0,0,\pi)),\\ &\qquad d(g_0,\,g_1\odot(0,0,\pi))\,,\,d(g_0\odot(0,0,\pi),\,g_1)\}\\ &= \min\{\,d(g_0,\,g_1)\,,\,d(g_0\odot(0,0,\pi),\,g_1)\}\end{aligned} \tag{4}$$

for all $q_i=(x_i,y_i,\theta_i)\in\mathrm{PT}(\mathbb{R}^2)$, $g_i=q_i=(x_i,y_i,\theta_i)\in\mathrm{SE}(2), i\in\{0,1\}$. Eq. (4) is due to $\gamma^*_{g_0\to g_1}(\tau)=\gamma^*_{\tilde g_1\to\tilde g_0}(1-\tau)$, with $\tilde g_i := g_i\odot(0,0,\pi)$, with $\gamma^*_{g_0\to g_1}$ a minimizing geodesic from $g_0=(\mathbf{x}_0,\theta_0)$ to $g_1=(\mathbf{x}_1,\theta_1)$, and **has 2 consequences:**
1) One can account for the $\mathrm{PT}(\mathbb{R}^2)$ structure in the building of the distance function before tracking takes place, cf. Prop. 1 below.
2) It affects cut-locus, the first Maxwell set (Prop. 2&3), and cusps (Prop. 4).
We apply a Riemannian limit [8, Thm.2] where $\overline{d}$ is approximated by Riemannian metric $\overline{d}^\epsilon$ induced by $\mathcal{G}^\epsilon_q(\dot q,\dot q) := \mathcal{G}_q(\dot q,\dot q)+\frac{\mathcal{C}^2(q)\,\xi^2}{\epsilon^2}\,|-\dot x\sin\theta+\dot y\cos\theta|^2$ for $\dot q=(\dot x,\dot y,\dot\theta), q=(x,y,\theta), 0<\epsilon\ll 1$, and use SR gradient $\mathcal{G}_q^{-1}\mathrm{d}W(q) := \mathcal{G}_q^{-1}P_{\Delta^*}\mathrm{d}W(q)=\frac{\mathcal{A}_1W(q)}{\xi^2\mathcal{C}^2(q)}\,\mathcal{A}_1|_q+\frac{\mathcal{A}_2W(q)}{\mathcal{C}^2(q)}\,\mathcal{A}_2|_q$ for steepest descent on $W=\overline{d}(\cdot,e)$.

Proposition 1. *Let $q\neq e$ be chosen such that there exists a unique minimizing geodesic $\gamma^*_\epsilon:[0,1]\to\mathrm{PT}(\mathbb{R}^2)$ of $\overline{d}^\epsilon(q,e)$ for $\epsilon\geq 0$ sufficiently small, that does not contain conjugate points (i.e. the differential of the exponential map of the Hamiltonian system is non-degenerate along γ^*_ϵ, cf. [15]). Then $\tau\mapsto\overline{d}(e,\gamma^*_0(\tau))$ is smooth and $\gamma^*_0(\tau)$ is given by $\gamma^*_0(\tau)=\gamma^*_b(1-\tau)$ with*

$$\begin{cases}\dot\gamma^*_b(\tau) = -W(q)\,(\mathcal{G}^{-1}_{\gamma^*_b(\tau)}\mathrm{d}W)(\gamma^*_b(\tau)), \quad \tau\in[0,1]\\ \gamma^*_b(0)=q,\end{cases} \tag{5}$$

with $W(q)$ the viscosity solution of the following boundary value problem:

$$\begin{cases}\mathcal{G}_q\left(\mathcal{G}_q^{-1}\mathrm{d}W(q),\,\mathcal{G}_q^{-1}\mathrm{d}W(q)\right)=1 \text{ for } q\neq e,\\ W(x,y,\pi)=W(x,y,0),\ \text{for all } (x,y)\in\mathbb{R}^2,\\ W(0,0,0)=W(0,0,\pi)=0.\end{cases} \tag{6}$$

Proof. By [8, Thm 2 and Thm 4], (extending [7, Thm 3.2] to non-uniform cost) we get minimizing SR geodesics in SE(2) by intrinsic gradient descent on W. The 2nd condition in (6) is due to $P^1=S^1/_\sim$, the 3rd is due to (4). When applying [8, Thm 4] we need differentiability of the SR distance. As our assumptions exclude conjugate and Maxwell-points, this holds by [16, Thm 11.15]. □

At least for $\epsilon=0$ and $\mathcal{C}=1$ the assumption in Prop. 1 on conjugate points is obsolete by [17] and [7, Thm 3.2, App.D].

3 Analysis of Maxwell sets for $\mathcal{C} = 1$

A *sub-Riemannian sphere* is a set of points equidistant from e. A sphere of radius R centred at e is given by $\mathcal{S}(R) = \{q \in \mathrm{PT}(\mathbb{R}^2) \,|\, \overline{d}(e,q) = R\}$. We define (the first) *Maxwell point* as a point in $\mathrm{PT}(\mathbb{R}^2)$ connected to e by multiple SR length minimizers. I.e. its *multiplicity* is > 1. All Maxwell points form a *Maxwell set*:

$$\mathcal{M} = \{q \in \mathrm{PT}(\mathbb{R}^2) \,|\, \exists\, \gamma^1, \gamma^2 \in \mathrm{Lip}([0,1], \mathrm{PT}(\mathbb{R}^2)),\ \text{s. t. } \dot{\gamma}^i \in \Delta|_{\gamma^i}\,,$$
$$\gamma^i(0) = e,\ \gamma^i(1) = q,\ \text{ for } i = 1,2,\ \text{and } \gamma^1 \neq \gamma^2,\ l(\gamma^1) = l(\gamma^2) = \overline{d}(e,q)\}.$$

The set $\mathcal{M}$ is a stratified manifold $\mathcal{M} = \bigcup_i \mathcal{M}_i$. We aim for maximal dimension strata: $\dim(\mathcal{M}_i) = 2$.

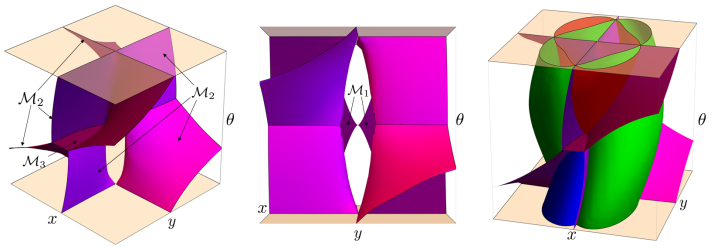

Fig. 1. Maxwell set and its intersection (right image) with the SR sphere in Fig. 2. The folds on the Green surface are in $\mathcal{M}_1$, the intersections of the Green surface with Red and Blue surface are in $\mathcal{M}_2$, the intersection of the Red and Blue surface is in $\mathcal{M}_3$.

Proposition 2. *Let $W(q) = \overline{d}(e,q)$ and let $W^{\mathrm{SE}(2)}(g) = d(e,g)$. The Maxwell set $\mathcal{M}$ is given by $\mathcal{M} = \bigcup_{i=1}^{3} \mathcal{M}_i$, see Fig. 1, where*

- *$\mathcal{M}_1$ is a part of local component of Maxwell set $\mathrm{Exp}(\mathrm{MAX}^2)$ in $\mathrm{SE}(2)$, see [18, Theorem 5.2], restricted by the condition $t_1^{\mathrm{MAX}} = W(\gamma(t_1^{\mathrm{MAX}}))$;*
- *$\mathcal{M}_2$ is given by $W^{\mathrm{SE}(2)}(g) = W^{\mathrm{SE}(2)}(g \odot (0,0,\pi))$;*
- *$\mathcal{M}_3$ is a part of global component of Maxwell set $\mathrm{Exp}(\mathrm{MAX}^5)$ in $\mathrm{SE}(2)$, see [18, Theorem 5.2], restricted by the condition $t_1^{\mathrm{MAX}} = W(\gamma(t_1^{\mathrm{MAX}}))$.*

Proof. There are two possible reasons for $\mathrm{PT}(\mathbb{R}^2) \ni q = g/_\sim$ be a Maxwell point: 1) if g is a Maxwell point in $\mathrm{SE}(2)$, s.t. $W^{\mathrm{SE}(2)}(g) = W(q)$ (i.e. $W^{\mathrm{SE}(2)}(g) \leq W^{\mathrm{SE}(2)}(g \odot (0,0,\pi))$); 2) if q is a (new) Maxwell point induced by the quotient (i.e. q is a root of $W^{\mathrm{SE}(2)}(g) = W^{\mathrm{SE}(2)}(g \odot (0,0,\pi))$). Strata $\mathcal{M}_1$, $\mathcal{M}_3$ follow from $\mathrm{Exp}(\mathrm{MAX}^2)$, $\mathrm{Exp}(\mathrm{MAX}^5)$ [18], while $\mathcal{M}_2$ is induced by $P^1 = S^1/_\sim$. Set $\mathcal{M}_3$ is in $\theta = 0$, as $\mathrm{Exp}(\mathrm{MAX}^5)$ is in $\theta = \pi$, which is now identified with $\theta = 0$.

Proposition 3. *The maximal multiplicity ν of a Maxwell point on a SR sphere depends on its radius R. Denote $\mathcal{M}^R = \mathcal{M} \cap \mathcal{S}(R)$ and $\mathcal{M}_i^R = \mathcal{M}_i \cap \mathcal{S}(R)$. One has the following development of Maxwell set as R increases, see Fig. 2:*

1. *if* $0 < R < \frac{\pi}{2}$ *then* $\mathcal{S}(R)$ *is homeomorphic to* S^2 *and it coincides with SR sphere in* $\mathrm{SE}(2)$, $\mathcal{M}^R = \mathcal{M}_1^R$ *and* $\nu = 2$;
2. *if* $R = \frac{\pi}{2}$ *then* $\mathcal{S}(R)$ *is homeomorphic to* S^2 *glued at one point,* $\mathcal{M}^R = \mathcal{M}_1^R \cup \mathcal{M}_2^R$, $\mathcal{M}_1^R \cap \mathcal{M}_2^R = \emptyset$, *and* $\nu = 2$;
3. *if* $\frac{\pi}{2} < R < \overline{R}$ *then* $\mathcal{S}(R)$ *is homeomorphic to* T^2, $\mathcal{M}^R = \mathcal{M}_1^R \cup \mathcal{M}_2^R$, $\mathcal{M}_1^R \cap \mathcal{M}_2^R = \emptyset$ *and* $\nu = 2$;
4. *if* $R = \overline{R} \approx \frac{17}{18}\pi$ *then* $\mathcal{S}(R)$ *is homeomorphic to* T^2, $\mathcal{M}^R = \mathcal{M}_1^R \cup \mathcal{M}_2^R$, *and* $\mathcal{M}_1^R$ *intersects* $\mathcal{M}_2^R$ *at four (conjugate) points,* $\nu = 2$;
5. *if* $\overline{R} < R < \tilde{R}$ *then* $\mathcal{S}(R)$ *is homeomorphic to* T^2, $\mathcal{M}^R = \mathcal{M}_1^R \cup \mathcal{M}_2^R$, *and* $\mathcal{M}_1^R$ *intersects* $\mathcal{M}_2^R$ *at four points, where* $\nu = 3$;
6. *if* $R = \tilde{R} \approx \frac{10}{9}\pi$ *then* $\mathcal{S}(R)$ *is homeomorphic to* T^2, $\mathcal{M} = \mathcal{M}_1^R \cup \mathcal{M}_2^R \cup \mathcal{M}_3^R$, $\mathcal{M}_1^R = \mathcal{M}_3^R$, *and* $\mathcal{M}_2^R$ *intersects* $\mathcal{M}_1^R$ *at two points, where* $\nu = 4$;
7. *if* $R > \tilde{R}$ *then* $\mathcal{S}(R)$ *is homeomorphic to* T^2, $\mathcal{M}^R = \mathcal{M}_2^R \cup \mathcal{M}_3^R$ *and* $\mathcal{M}_2^R$ *intersects* $\mathcal{M}_3^R$ *at four points, where* $\nu = 3$.

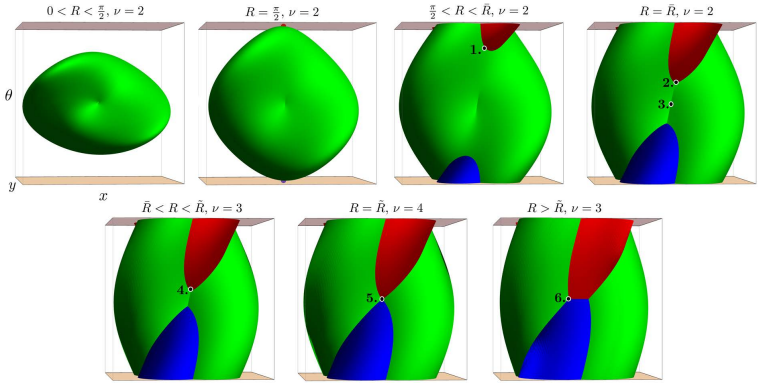

Fig. 2. Evolution of the 1st Maxwell set as the radius R of the SR-spheres increases.

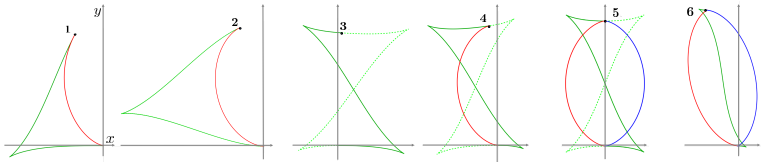

Fig. 3. SR length minimizers ending at the points indicated at Fig. 2.

Remark 1. Results in [19, Sec.4] imply that $\tilde{R}$ can be computed from the system:

$$\tilde{R}/2 = K(k_1) = k_2\, p_1(k_2), \quad \frac{K(k_1) - E(k_1)}{k_1\sqrt{1-k_2^2}} = \frac{p_1(k_2) - \mathrm{E}(p_1(k_2), k_2)}{\mathrm{dn}(p_1(k_2), k_2)}, \tag{7}$$

where $K(k)$ and $E(k)$ are complete elliptic integrals of the 1st and 2nd kind; $\mathrm{E}(u,k) = E(\mathrm{am}(u,k),k)$, while $E(v,k)$ is the incomplete elliptic integral of the

2nd kind and $\mathrm{am}(u,k)$ is the Jacobian amplitude; $p_1(k)$ is the first positive root of $\mathrm{cn}(p,k)(\mathrm{E}(p,k)-p)-\mathrm{dn}(p,k)\,\mathrm{sn}(p,k)=0$; and $\mathrm{sn}(p,k)$, $\mathrm{cn}(p,k)$, $\mathrm{dn}(p,k)$ are Jacobian elliptic functions. Solving (7), we get $\tilde{R}\approx 1.11545\,\pi\approx 10/9\,\pi$. Radius $\overline{R}$ is s.t. $\mathcal{S}(\bar{R})$ hits the 1st conjugate set and can be computed as well.

4 Set of Reachable End Conditions by Cuspless Geodesics

A *cusp point* $\mathbf{x}(t_0)$ on a spatial projection of a (SR) geodesic $t\mapsto(\mathbf{x}(t),\theta(t))$ in $\mathbb{R}^2\times S^1$ is a point where the only spatial control switches sign, i.e. $u^1(t_0):=\dot{x}(t_0)\cos\theta(t_0)+\dot{y}(t_0)\sin\theta(t_0)=0$ and $(u^1)'(t_0)\neq 0$. In fact, the 2nd condition $(u^1)'(t_0)\neq 0$ is obsolete [8, App.C]. The next proposition shows that the occurrence of cusps is greatly reduced in $\mathbb{R}^2\times P^1$.

Let $\mathfrak{R}\subset\mathbb{R}^2\times S^1$ denote the set of endpoints that can be connected to the origin $e=(0,0,0)$ by a SR geodesic $\gamma:[0,T]\to\mathbb{R}^2\times S^1$ whose spatial control $u^1(t)>0$ for all $t\in[0,T]$. Let $\tilde{\mathfrak{R}}\subset\mathbb{R}^2\times P^1$ denote the set of endpoints that can be connected to e by a SR geodesic $\gamma:[0,T]\to\mathbb{R}^2\times S^1$ whose spatial control $u^1(t)$ does not switch sign for all $t\in[0,T]$. Henceforth, such a SR geodesic whose spatial control $u^1(\cdot)$ does not switch sign will be called 'cuspless' geodesic.

Proposition 4. *The set of reachable end-conditions in $\mathbb{R}^2\times P^1$ via 'cuspless' SR geodesics departing from $e=(0,0,0)$ is given by*

$$\begin{aligned}\tilde{\mathfrak{R}}=\{(x,y,\theta)\in\mathrm{PT}(\mathbb{R}^2)\mid{}&(x,y,\theta)\in\mathfrak{R}\quad \textit{or}\ \ (x,y,\theta+\pi)\in\mathfrak{R}\\ &\textit{or}\ \ (-x,y,-\theta)\in\mathfrak{R}\ \ \textit{or}\ \ (-x,y,-\theta+\pi)\in\mathfrak{R}\ \ \textit{or}\ x=y=0\}.\end{aligned}\tag{8}$$

Proof. A point $(x,y,\theta)\in\mathbb{R}^2\times P^1$ can be reached with a 'cuspless' SR geodesic if 1) $(x,y,\theta)\in\mathbb{R}^2\rtimes S^1$ can be reached with a 'cuspless' SR geodesic in SE(2) or 2) if $(-x,y,-\theta)$ can be reached with a 'cuspless' SR geodesic in SE(2). Recall from [20, Thm.7] that $(x,y,\theta)\in\mathfrak{R}\Rightarrow(x\geq 0$ and $(x,y)\neq(0,0))$. If $x\geq 0$ and $(x,y)\neq(0,0)$, the first option holds if $(x,y,\theta)\in\mathfrak{R}$, and the second option holds if $(x,y,\theta+\pi)\in\mathfrak{R}$. If $x<0$, the endpoint can only be reached by a 'cuspless' SR geodesic in SE(2) with a negative spatial control function $u^1<0$. Here we rely on symmetry $(x,y,\theta)\mapsto(-x,y,-\theta)\Rightarrow(x(t),y(t),\theta(t))\mapsto(-x(t),y(t),-\theta(t)))$ that holds for SR geodesics $(x(\cdot),y(\cdot),\theta(\cdot))$ in SE(2). For the control u^1 in (2), this symmetry implies $u^1(t)\mapsto -u^1(t)$. By [20, Thm.10] one has $(x,y,\theta)\in\mathfrak{R}\Rightarrow(x,y,\theta+\pi)\notin\mathfrak{R}$, and points with $x=y=0$ are not in $\mathfrak{R}$ [20, Remark 5.5] so all 'or' conditions in (8) are exclusive. □

Set $\mathfrak{R}$ yields a single cone field of reachable angles in $x>0$, see [20, fig 14, thm 9]. By Prop. 4, set $\tilde{\mathfrak{R}}$ is a union of 2 such cone fields that is also reflected to $x<0$.

5 Practical Advantages in Vessel Tracking

Distance $W(q)$ can be numerically obtained by solving the eikonal PDE of Eq. (6) via similar approaches as was previously done for the SE(2) case. E.g., via an iterative upwind scheme [7], or a fast marching (FM) solver [21] in which case the SR metric tensor is approximated by an anisotropic Riemannian metric tensor [22]. A gradient descent (cf. Eq. (5)) on W then provides the SR geodesics.

We construct the cost function $\mathcal{C}$ in the same way as in [7]: (1) a retinal image is lifted via the orientation score transform using cake wavelets [23]; (2) vessels are enhanced via left-invariant Gaussian derivatives using $\mathcal{A}_3$; (3) a cost function is constructed via $\mathcal{C} = \frac{1}{1+\lambda \mathcal{V}^p}$, with $\mathcal{V}$ the max-normalized vessel enhanced orientation score, and with λ and p respectively a "cost-strength" and contrast parameter. We use the same data and settings ($\lambda = 100$, $p = 3$ and $\xi = 0.01$) as in [7], and perform vessel tracking on 235 vessel segments. For the results on all retinal image patches, see http://erikbekkers.bitbucket.io/PTR2.html.

Fig. 4 shows the results on three different vessel segments with comparison between SR geodesics in SE(2) and PT($\mathbb{R}^2$). As expected, with the PT($\mathbb{R}^2$) model we always obtain the SE(2) geodesic with minimum SR length (cf. Eq. (4)). This has the advantage that overall we encounter less cusps in the tracking. Additionally, the PT($\mathbb{R}^2$) model is approximately four times faster since now we only have to consider half of the domain $\mathbb{R}^2 \times S^1$, and by Prop. 1 we only run once (instead of twice). The average computation time via FM for constructing W with the SE(2) model for 180×140 pixel patches is 14.4 seconds, whereas for the PT($\mathbb{R}^2$) model this is only 3.4 seconds. The rightmost image in Fig. 4 shows an exceptional case in which the reversed boundary condition (red arrow) is preferred as this leads to a geodesic with only one cusp instead of two.

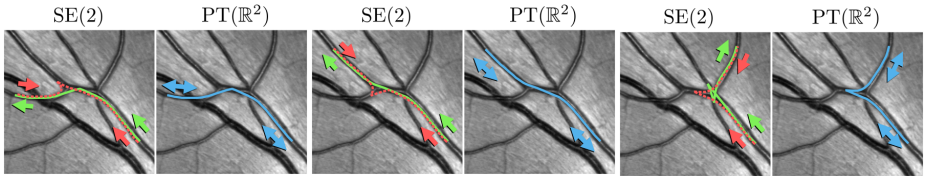

Fig. 4. Data-adaptive SR geodesics in SE(2) (in green and red-dashed) compared to SR geodesics in PT($\mathbb{R}^2$) (in blue). For the SE(2) case we specify antipodal boundary conditions since the correct initial and end directions are not known a priori.

6 Conclusion

We have shown the effect of including the projective line bundle structure SR in optimal geodesic tracking (Prop. 1), in SR geometry (Prop. 2), and in Maxwell-stratification (Prop. 3), and in the occurrence of cusps in spatially projected geodesics (Prop. 4). It supports our experiments that show benefits of including such a projective line bundle structure: A better vessel tracking algorithm with a reduction of cusps and computation time. As the cusp-free model without reverse gear [8] also benefits [8, Fig.12] from PT($\mathbb{R}^2$)-structure, we leave the Maxwell stratification of this combined model for future work.

References

1. G. Peyré, M. Péchaud, R. Keriven, L.D. Cohen, *Geodesic methods in computer vision and graphics*, Foundations and Trends in Computer Graphics and Vision, 5(34), 197–397, 2010.

2. V. Caselles, R. Kimmel, G. Sapiro, *Geodesic Active Contours*, IJCV, 22(1), 61–79, 1997.
3. L. Cohen, R. Kimmel, *Global minimum for active contour models*, IJCV, 24(1), 57–78, 1997.
4. M. Péchaud, R. Keriven, G. Peyré, *Extraction of tubular structures over an orientation domain*, In IEEE conf. on CVPR, 336–342, 2009.
5. E.J. Bekkers, *Retinal Image Analysis using Sub-Riemannian Geometry in SE(2)*, PhD thesis, Eindhoven University of Technology, Biomedical Engineering, 2017.
6. D. Chen, *New Minimal Path Models for Tubular Structure Extraction and Image Segmentation*, PhD thesis, Universite Paris Dauphine, PSL Research Univ., 2016.
7. E.J. Bekkers, R. Duits, A. Mashtakov, G. Sanguinetti, *A PDE approach to data-driven sub-riemannian geodesics in SE(2)*, SIAM-SIIMS, 8(4), 2740–2770, 2015.
8. R. Duits, S. Meesters, J. Mirebeau, J. Portegies, *Optimal paths for variants of the 2d and 3d Reeds-Shepp car with applications in image analysis*, (*arXiv:1612.06137*), 2017.
9. J. Zhang, B. Dashtbozorg, E. Bekkers, J. Pluim, R. Duits, B. ter Haar Romeny, *Robust retinal vessel segmentation via locally adaptive derivative frames in orientation scores*, IEEE TMI, 35 (12), 2631–2644, 2016.
10. G. Citti, A. Sarti, *A cortical based model of perceptual completion in the roto-translation space*, JMIV, 24(3), 307–326, 2006.
11. J. Petitot, *Vers une Neuro-gèométrie. Fibrations corticales, structures de contact et contours subjectifs modaux*, Math. Inf. Sci. Humaines, 145, 5-101, 1999.
12. U. Boscain, R. Duits, F. Rossi, Y. Sachkov, *Curve cuspless reconstruction via sub-Riemannian geometry*, ESAIM:COCV, 20, 748–770, 2014.
13. A.P. Mashtakov, A.A. Ardentov, Y.L. Sachkov, *Parallel algorithm and software for image inpainting via sub-Riemannian minimizers on the group of rototranslations*, NMTMA, 6(1), 95–115, 2013.
14. S. Abbasi-Sureshjani, J. Zhang, R. Duits, B. ter Haar Romeny, *Retrieving challenging vessel connections in retinal images by line co-occurence statistics*, Biological Cybernetics, 111(3), 237-247, 2017.
15. A.A. Agrachev, Yu.L. Sachkov, *Control Theory from the Geometric Viewpoint*, Springer-Verlag, 2004.
16. A.A. Agrachev, D. Barilari, U. Boscain, *Introduction to Riemannian and Sub-Riemannian Geometry from the Hamiltonian Viewpoint*, preprint SISSA 09/2012/M november 20, 2016.
17. Y.L. Sachkov, *Conjugate and cut time in the sub-Riemannian problem on the group of motions of a plane*, ESAIM:COCV, 16(4), 1018–1039, 2009.
18. I. Moiseev, Y. L. Sachkov, *Maxwell strata in sub-Riemannian problem on the group of motions of a plane*, ESAIM:COCV, 16(2), 380–399, 2010.
19. Yu.L. Sachkov, *Cut locus and optimal synthesis in the sub-Riemannian problem on the group of motions of a plane*, ESAIM:COCV, 17(2), 293–321, 2011.
20. R. Duits, U. Boscain, F. Rossi, Y. Sachkov, *Association fields via cuspless sub-Riemannian geodesics in SE(2)*, JMIV, 49(2), 384–417, 2014.
21. J.-M. Mirebeau, *Anisotropic Fast-Marching on cartesian grids using Lattice Basis Reduction*, SIAM J. Num. Anal., 52(4), 1573–1599, 2014.
22. G. Sanguinetti, E.J. Bekkers, R. Duits, M.H.J. Janssen, A. Mashtakov, J.-M. Mirebeau, *Sub-Riemannian fast marching in SE(2)*, LNCS, 366–374, 2015.
23. R. Duits, M. Felsberg, G. Granlund, B.M. ter Haar Romeny, *Image analysis and reconstruction using a wavelet transform constructed from a reducible representation of the Euclidean motion group*, IJCV, 72(1), 79–102, 2007.

Vessel Tracking on the Projective Line Bundle

Erik Bekkers & Remco Duits & Alexey Mashtakov & Yuri Sachkov

TU/e Eindhoven & PSI Pereslavl-Zalessky

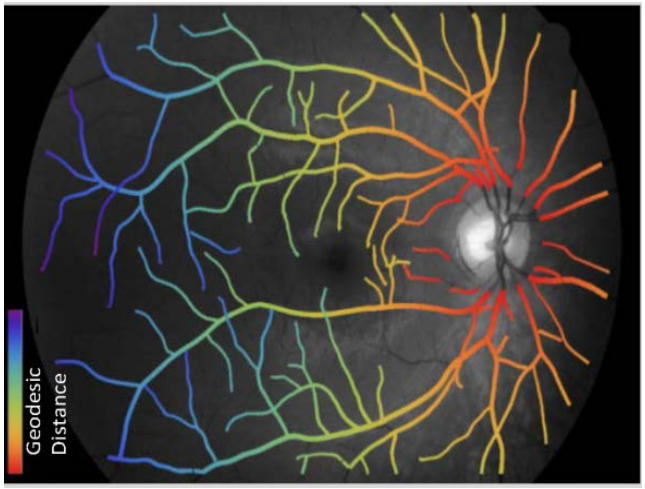

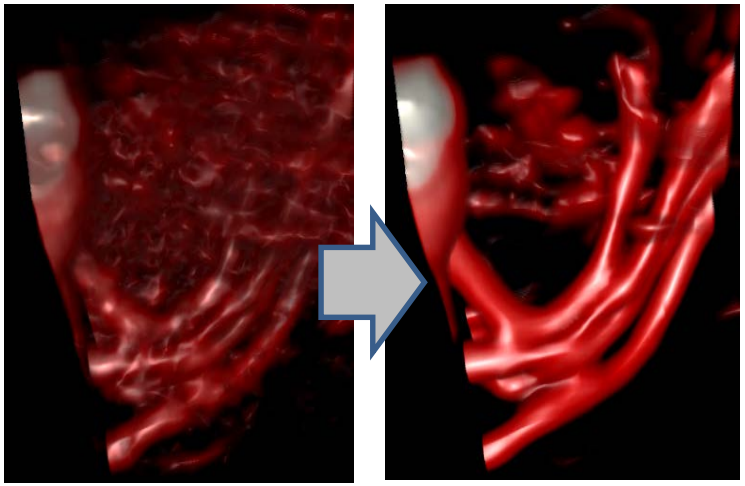

Project: ERC Lie Analysis 335555

Project: Russian Science Foundation 17-11-01387

Orientation Scores - Background

- Elongated structures appear in many medical images

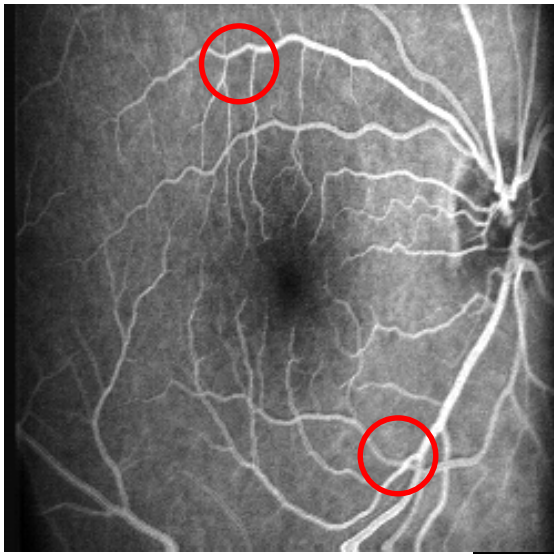

Retina

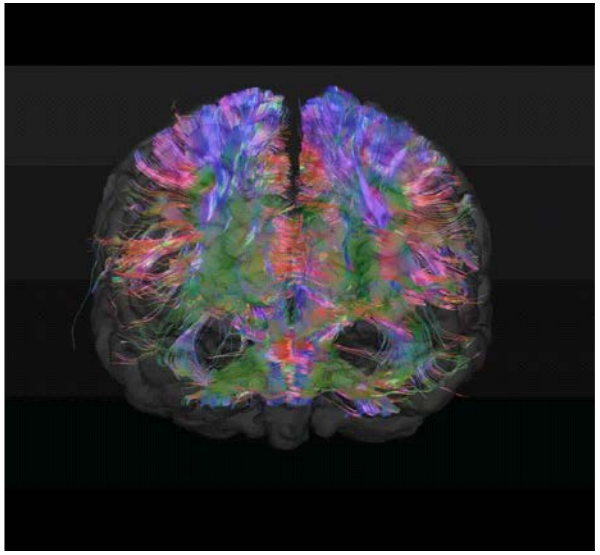

Brain White Matter

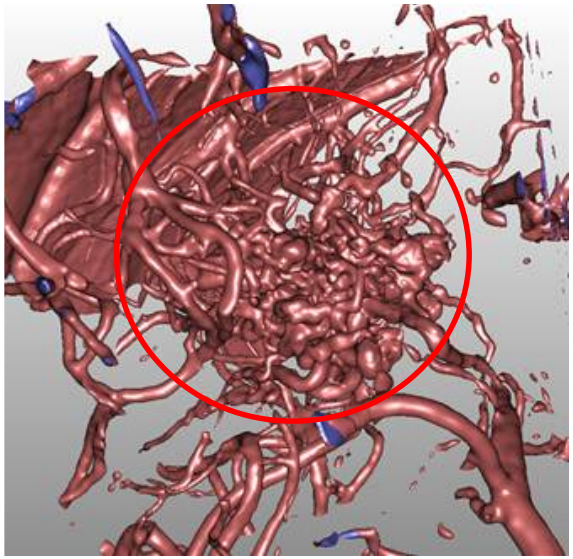

Vessels in brain

- Current detection and enhancement often fails at crossings/bifurcations etc.

→ a costly increase of user-interaction in tracking tools for computer aided diagnosis & therapy planning

Solution: Extend the Domain of Images

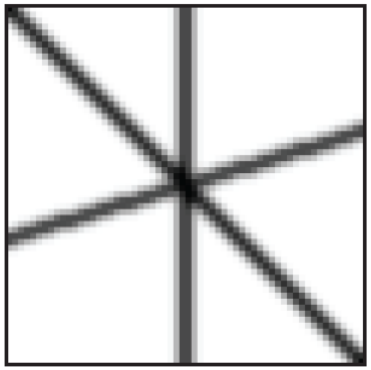

$f(\mathbf{x})$

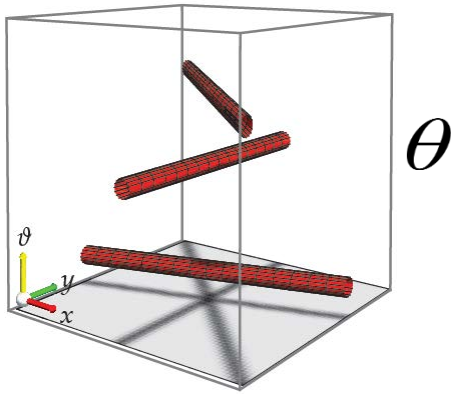

$U(\mathbf{x}, \theta)$

1.) For crossing-preserving diffusions:

original on image via invertible score

Solution: Extend the Domain of Images

2.) For correct tracking at crossings and bifurcations:

Vessel tracking in 2D X-ray angiogram

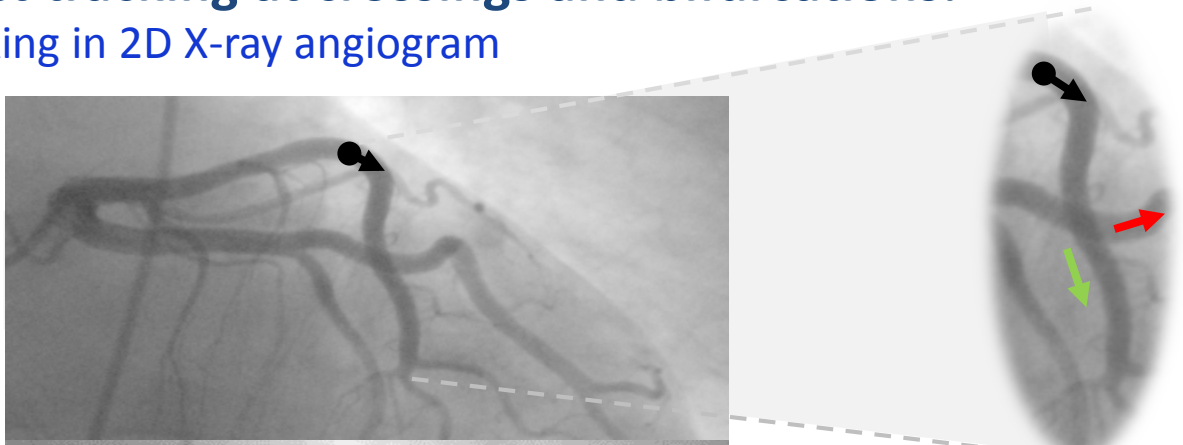

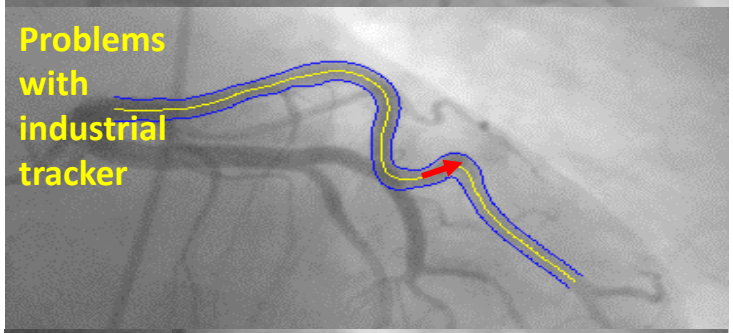

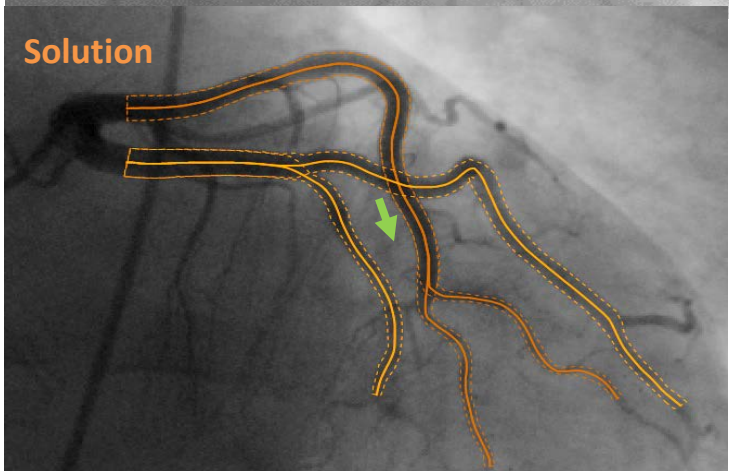

Vessel tracking in orientation scores

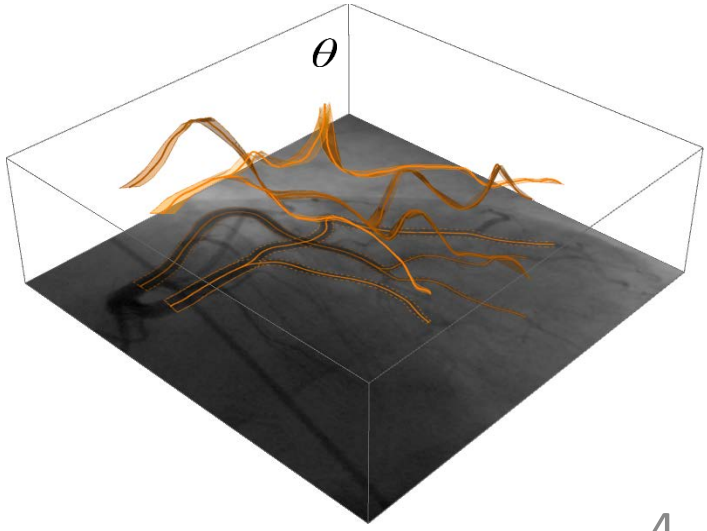

Processing via Orientation Scores

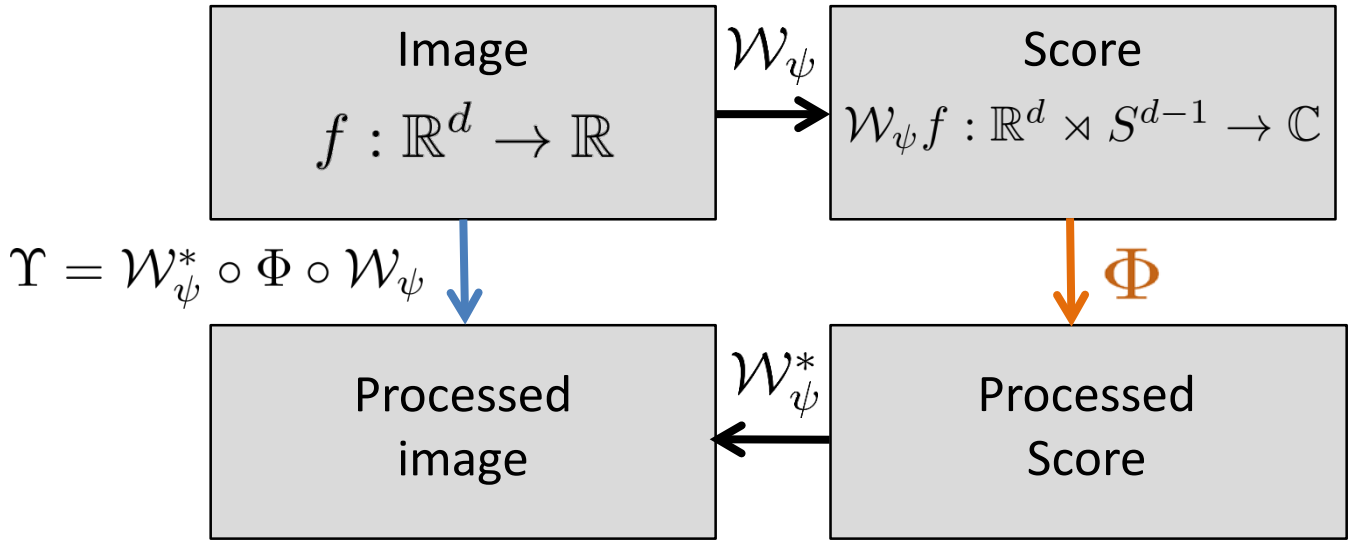

- Design of ψ for invertible transformation $\mathcal{W}_\psi$
- Design of LEFT-INVARIANT operators Φ in the score domain

A. Tracking via Globally Optimal Geodesics

B. Nonlinear Diffusions

Lie Group Analysis via Invertible Scores

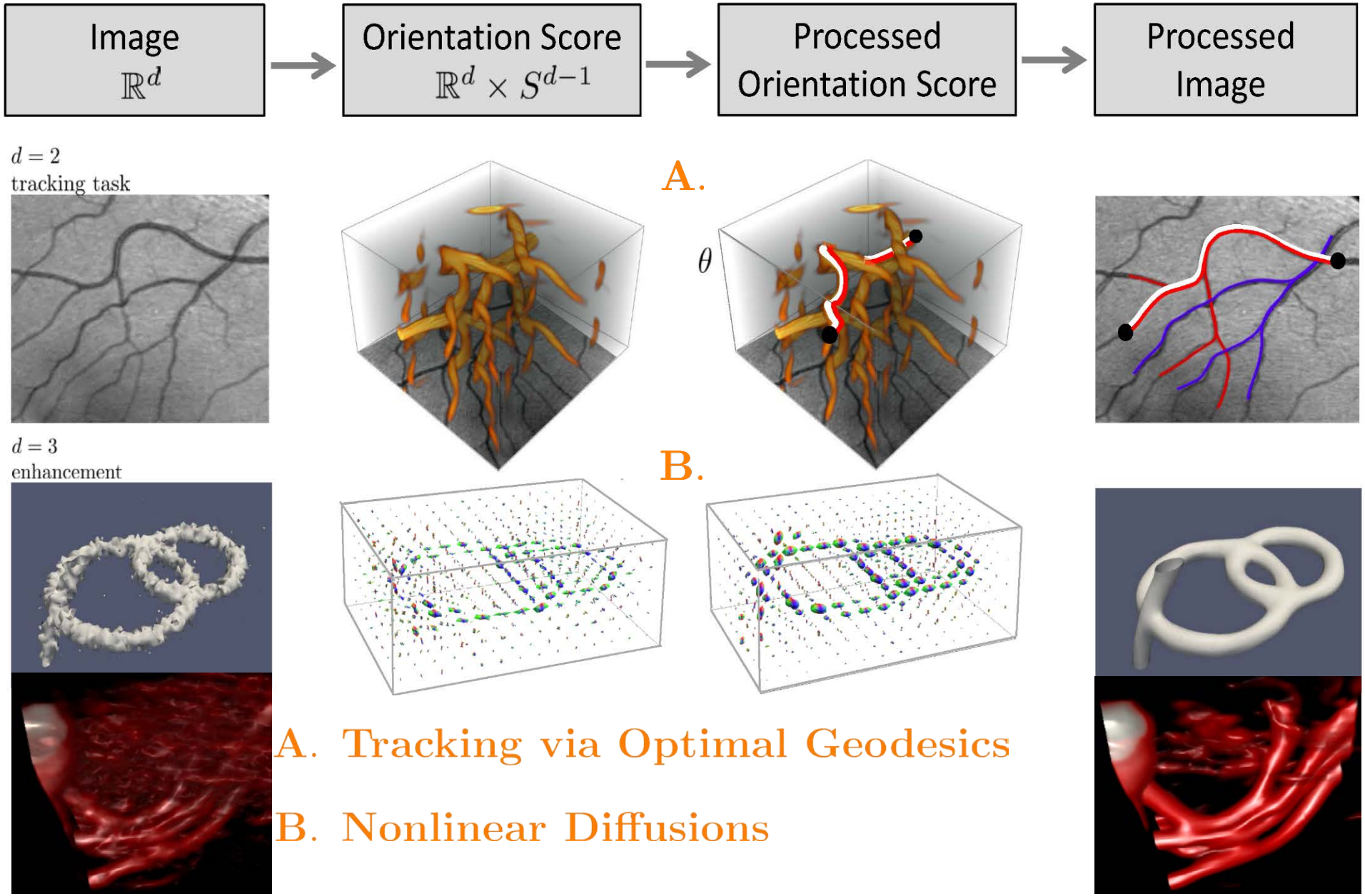

Both by Left-invariant PDE's on Orientation Scores

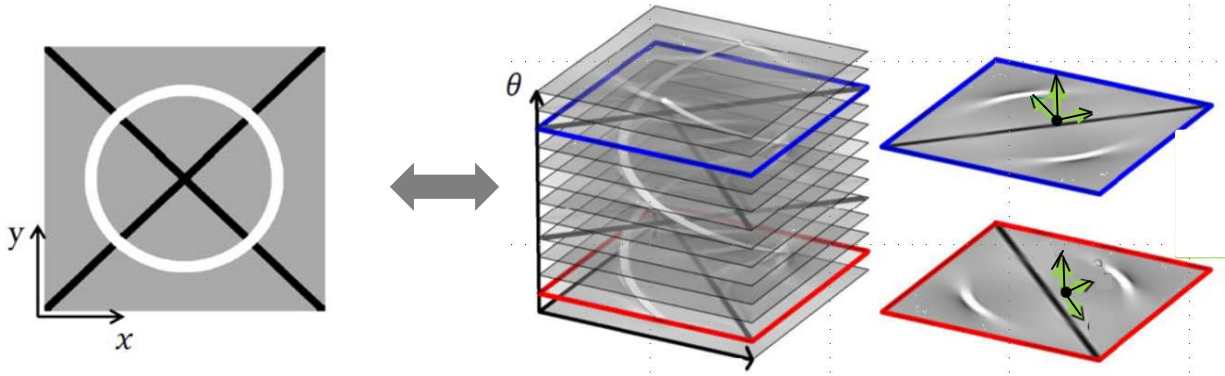

Moving frame

$$\begin{aligned}\mathcal{A}_1 &= \cos\theta\,\partial_x + \sin\theta\,\partial_y\\ \mathcal{A}_2 &= -\sin\theta\,\partial_x + \cos\theta\,\partial_y\\ \mathcal{A}_3 &= \partial_\theta\end{aligned}$$

A. Tracking: via Steepest Descent on Wavefronts in score via eikonal PDE

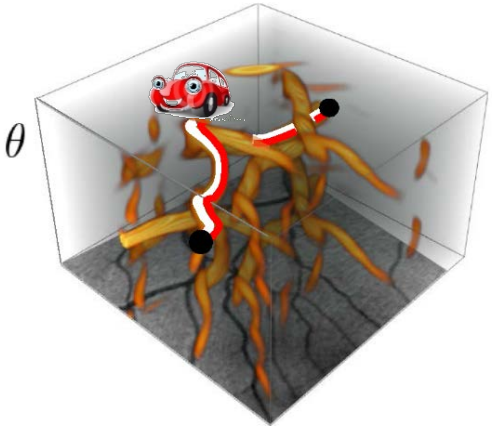

$$\begin{cases}\mathcal{F}^*(\mathbf{p},\mathrm{d}U(\mathbf{p})) = \sqrt{\sum_{i,j=1}^{n} g^{ij}(\mathbf{p})\mathcal{A}_i U(\mathbf{p})\mathcal{A}_j U(\mathbf{p})} = 1, & \mathbf{p}=(\mathbf{x},\mathbf{n}) \in \mathbb{M}\setminus S,\\ U(\mathbf{p}) = 0, & \mathbf{p}\in S \text{ (source set)}\end{cases}$$

$\mathcal{F}$ puts costs on the "car"  controls:

- spatial velocity
- angular velocity

B. Enhancement: Evolutions on score

$$\begin{cases}\frac{\partial W}{\partial t} = \sum_{i=1}^{n} -a^i\mathcal{A}_i W + \sum_{i,j=1}^{n}\mathcal{A}_i(D^{ij}\mathcal{A}_j W) \mp \sum_{i,j=1}^{n} g^{ij}\mathcal{A}_i W\cdot\mathcal{A}_j W\\ W|_{t=0} = \mathcal{W}_\psi f\end{cases}$$

A: Data-Adaptive Geodesic Tracking in Orientation Scores

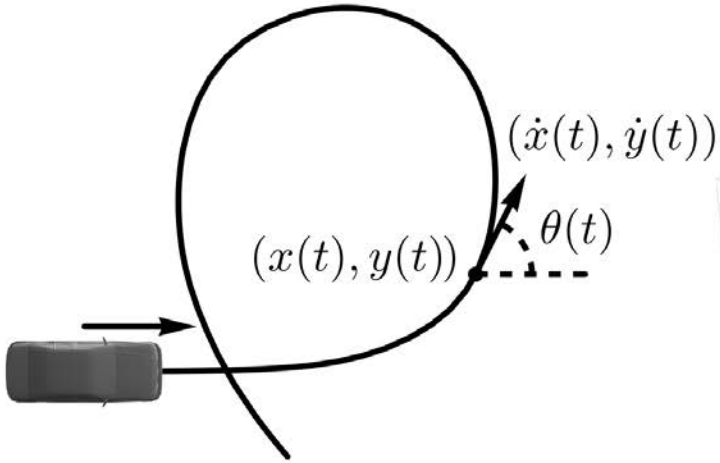

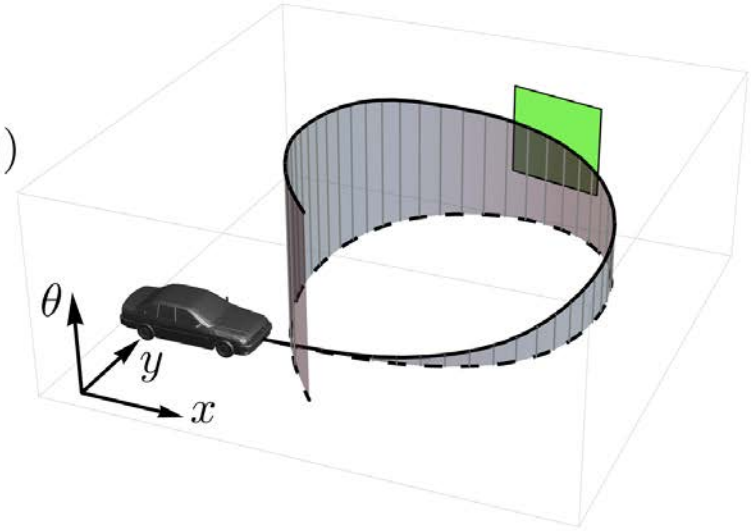

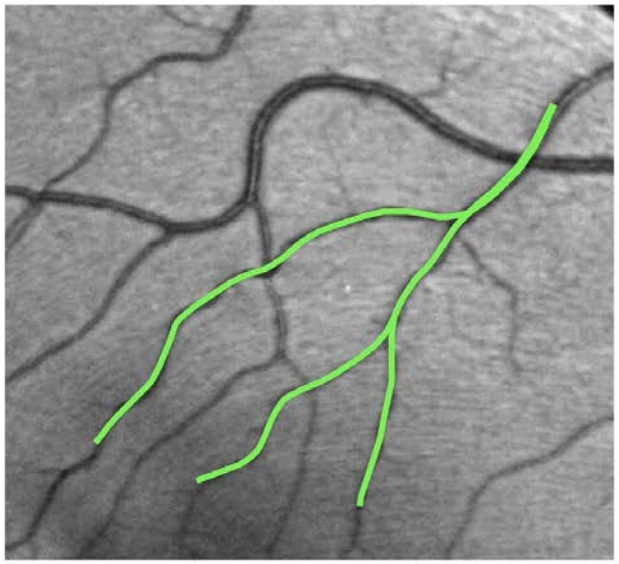

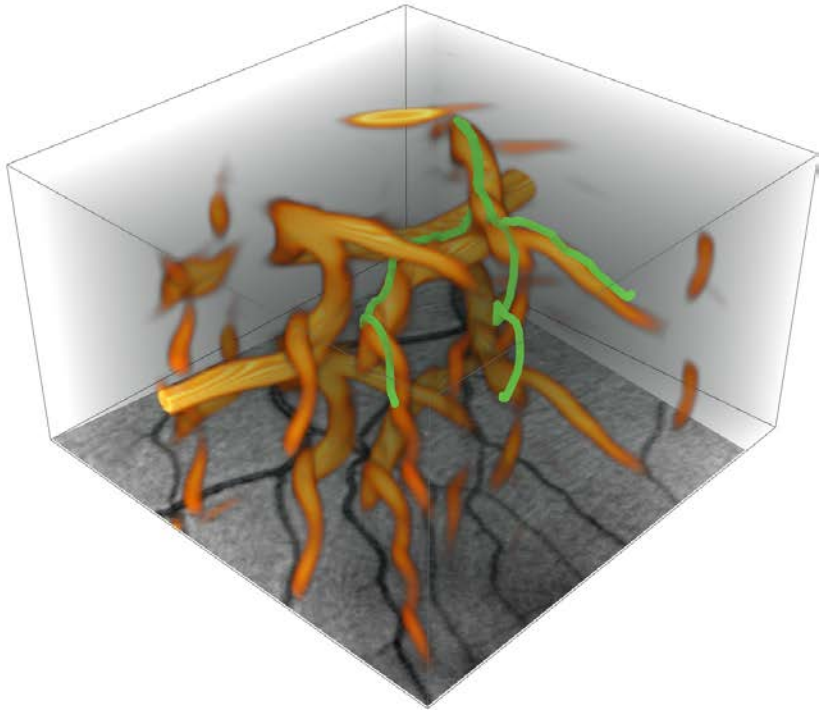

Vessel tracking

Standard 2D shortest paths

Standard shortest paths in $SE(2)$

Sub-Riemannian shortest paths in $SE(2)$

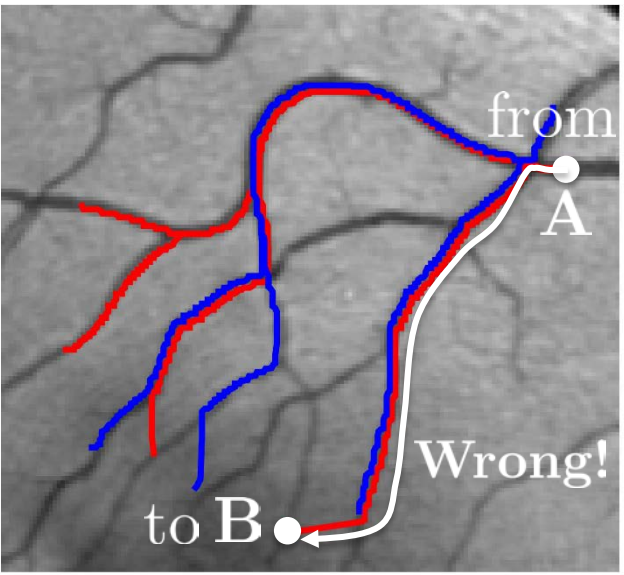

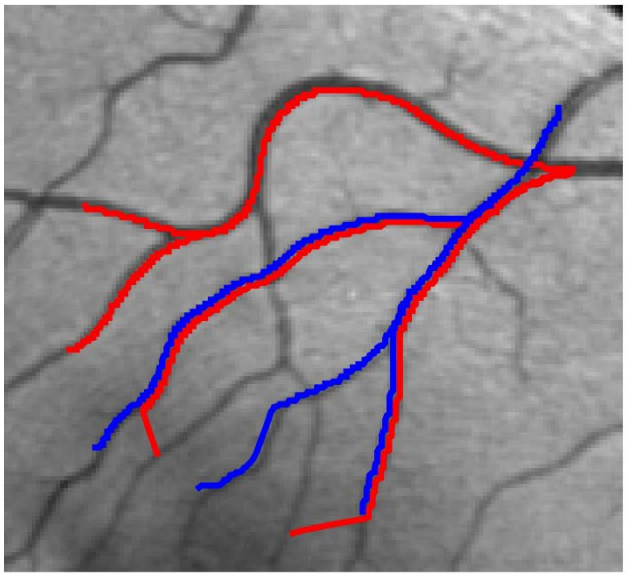

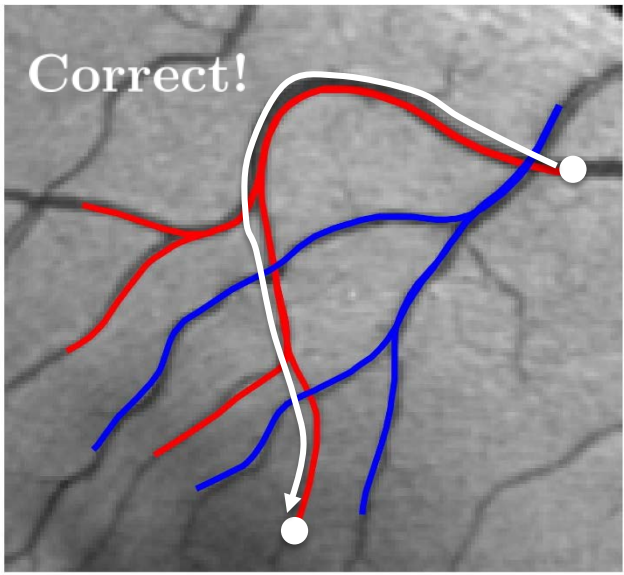

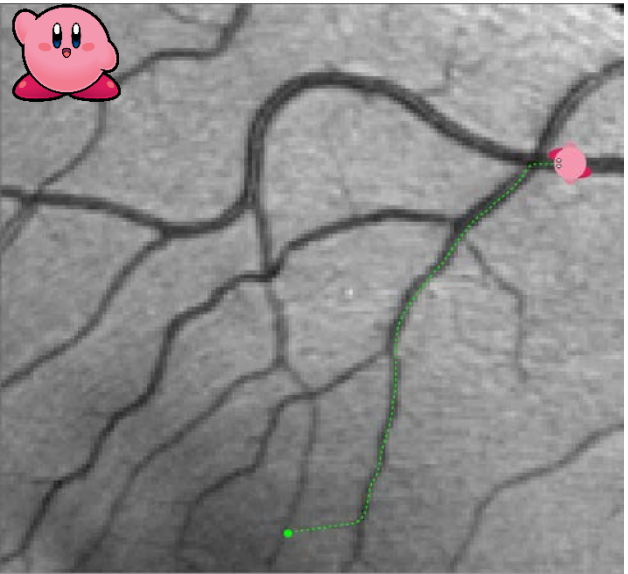

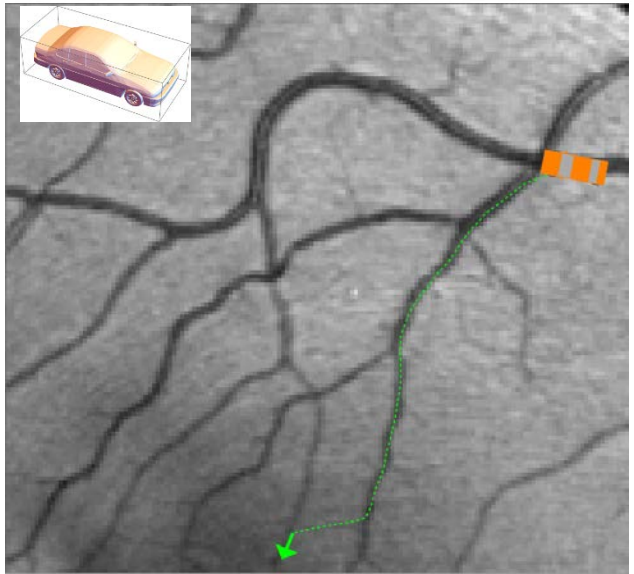

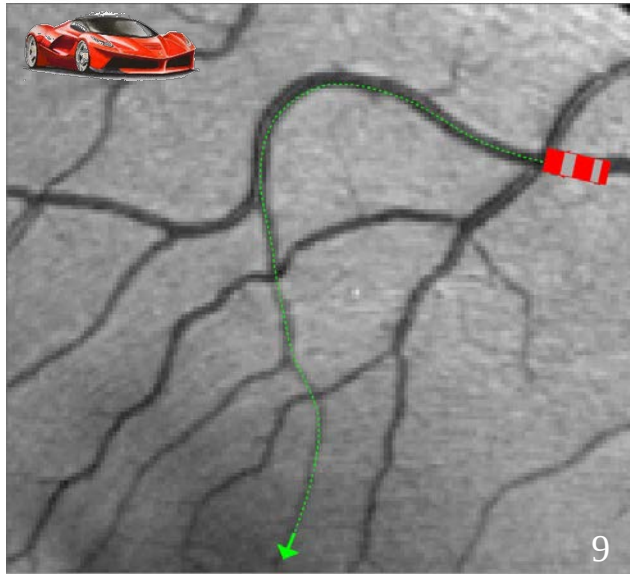

First Geodesic Wavefronts in Orientation Scores

via orientation scores
no leakage:

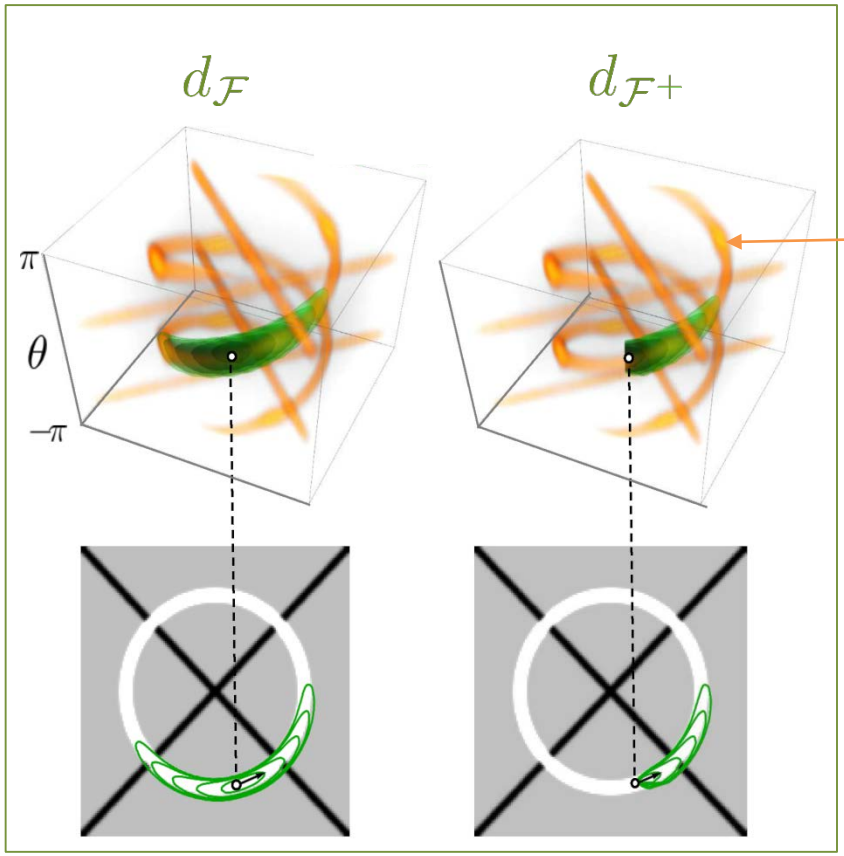

conventional leakage:

Finsler Function Reeds-Shepp car with mobility & reverse gear:

$$\mathcal{F}(\dot{\mathbf{x}},\dot{\mathbf{n}}) = \begin{cases} \mathcal{C}(\mathbf{x},\mathbf{n})\sqrt{\xi^2|(\dot{\mathbf{x}}\cdot\mathbf{n})|^2 + \|\dot{\mathbf{n}}\|^2} & \text{if } \dot{\mathbf{x}}\wedge\mathbf{n}\neq 0 \\ \infty & \text{else} \end{cases}$$

Finsler Function Reeds-Shepp car without reverse gear

$$\mathcal{F}^{+}(\dot{\mathbf{x}},\dot{\mathbf{n}}) = \begin{cases} \mathcal{C}(\mathbf{x},\mathbf{n})\sqrt{\xi^2|\dot{\mathbf{x}}\cdot\mathbf{n})|^2 + \|\dot{\mathbf{n}}\|^2} & \text{if } \dot{\mathbf{x}}\wedge\mathbf{n}\neq 0 \text{ and } \mathbf{x}\cdot\mathbf{n}\geq 0 \\ \infty & \text{else} \end{cases}$$

Tracking Globally Optimal Geodesics in Orientation Scores

Quasi-distance on $\mathbb{M} = \mathbb{R}^d \rtimes S^{d-1}$

$$d_{\mathcal{F}}(\mathbf{p}_S, \mathbf{p}) = \min_{\substack{\gamma \in \mathrm{Lip}([0,1],\mathbb{M}),\\ \gamma(0)=\mathbf{p}_S, \gamma(1)=\mathbf{p}}} \int_0^1 \mathcal{F}(\gamma(t), \dot{\gamma}(t))\,\mathrm{d}t.$$

$$\mathcal{F}^*(\mathbf{p}, \hat{\mathbf{p}}) = \sup_{\dot{\mathbf{p}} \in T_{\mathbf{p}}\mathbb{M}} \frac{\langle \hat{\mathbf{p}}, \dot{\mathbf{p}} \rangle}{\mathcal{F}(\mathbf{p}, \dot{\mathbf{p}})}$$

1. Set up PDE

$$\begin{cases} \mathcal{F}^*(\mathrm{d}U(\mathbf{p})) = 1, & \mathbf{p} \in \mathbb{M} \setminus S, \\ U(\mathbf{p}) = 0, & \mathbf{p} \in S \end{cases}$$

2. Derive **viscosity solution** $\mathrm{U(p)}$
   - Fast-Marching Mirebeau 2014
   - Iterative PDE method

3. Apply Back-tracking

$$\begin{cases} \dot{\gamma}(t) = U(\mathbf{p}) \cdot \mathrm{d}_{\hat{\mathbf{p}}}\mathcal{F}^*(\gamma(t), \mathrm{d}U(\gamma(t))), \\ \gamma(0) = \mathbf{p}_S, \quad \gamma(1) = \mathbf{p}. \end{cases}$$

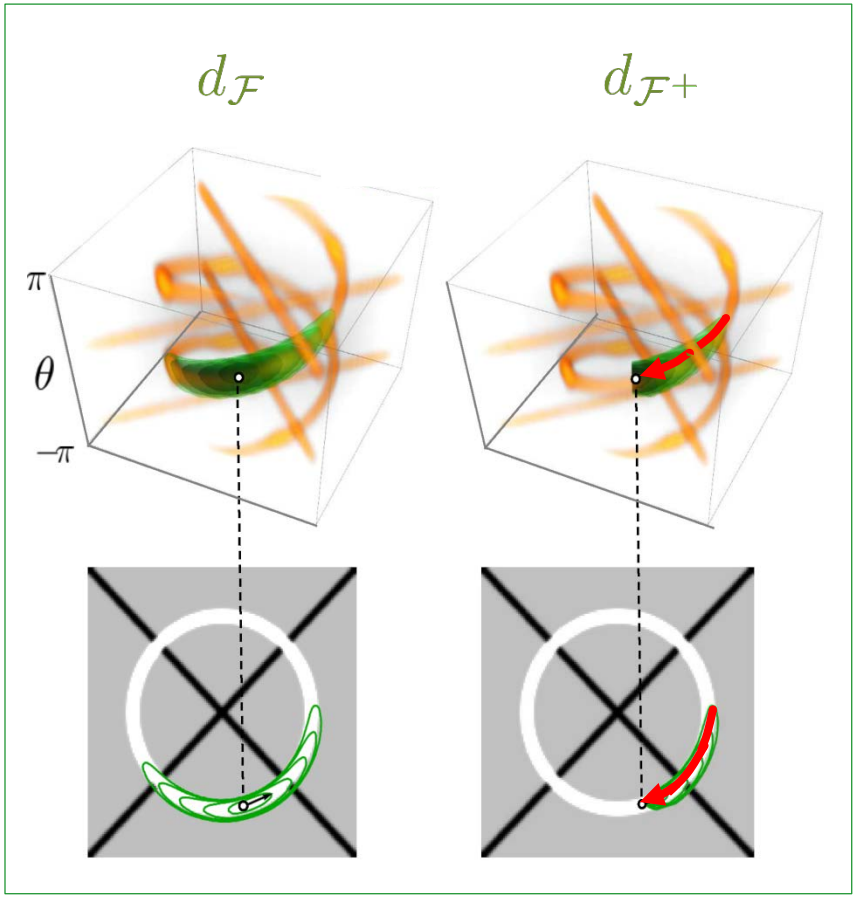

The Reeds Shepp Car with and without Reverse Gear

Sub-Riemannian

With reverse gear

control sets.

Asymmetric Version

Without reverse gear

control sets.

Bekkers Duits Mashtakov Sanguinetti SIIMS 2016

Duits Meesters Mirebeau Portegies JMIV 2017

The Cones of Reachable Angles without Cusps

Analytic Description cones:

1) Duits Boscain Rossi Sachkov JMIV 2014

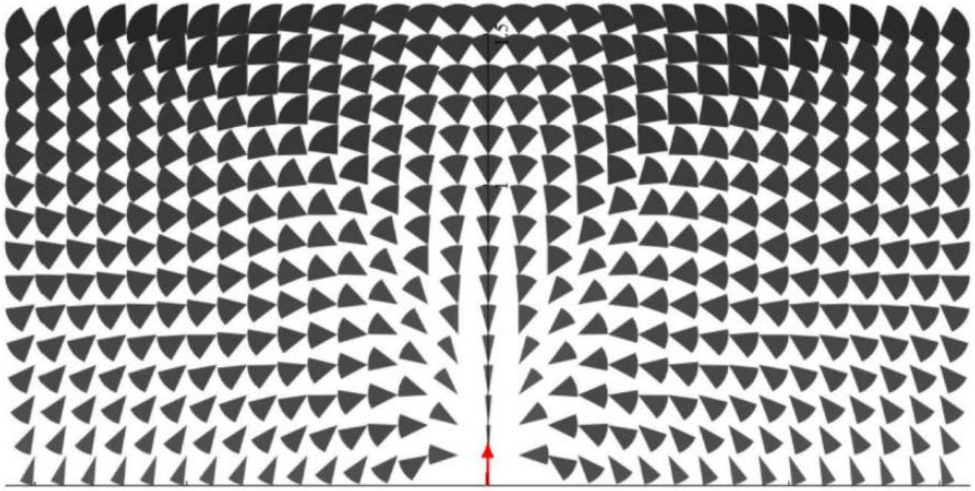

2) Duits Ghosh D.Haije Mashtakov JDCS 2016

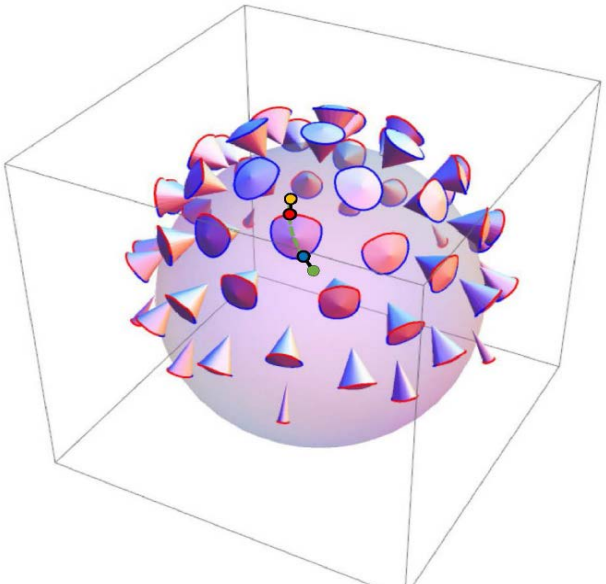

Optimal Synthesis (!) SR-Problem on SE(2):

Sachkov COCV 2010

$$t_{\text{cut}} \geq t_{\text{cusp}}$$

Boscain Duits Rossi Sachkov COCV 2014

SR-geodesics in the Projective Line Bundle

Importance stressed by **Petitot 1999 & Boscain 2010** for cortical
We use it for vessel tracking & analysis:

$$P^1 = S^1/_{\sim}$$

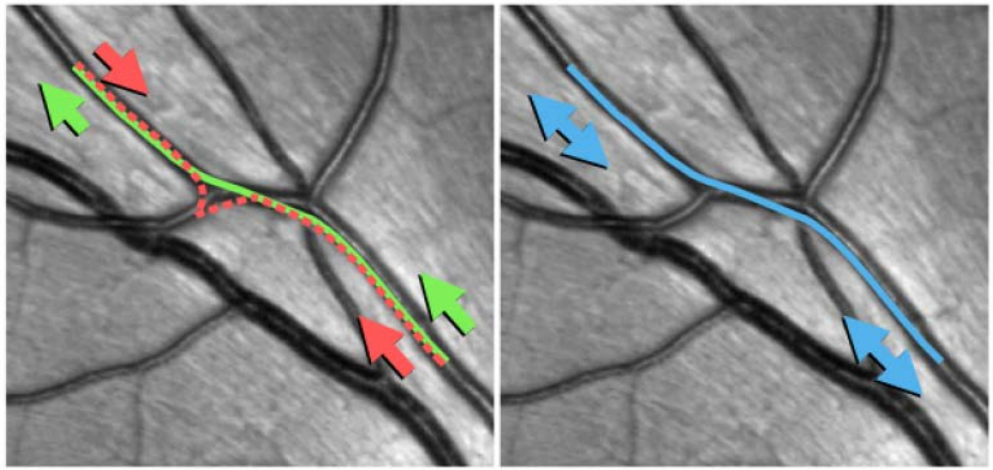

$$\overline{d}(q_0, q_1) = \min\{ d(g_0, g_1), d(g_0 \odot (0,0,\pi), g_1)\}$$

1) One can account for the $\mathrm{PT}(\mathbb{R}^2)$ structure in the building of the distance function before tracking takes place
2) It affects cut-locus, the first Maxwell set and reduces cusps

Accounting for the Projective Line Bundle is Simple

Proposition 1. *Let $q \neq e$ be chosen such that there exists a unique minimizing geodesic $\gamma_\epsilon^* : [0,1] \to \mathrm{PT}(\mathbb{R}^2)$ of $\overline{d}^{\epsilon}(q,e)$ for $\epsilon \geq 0$ sufficiently small, that does not contain conjugate points.*
Then $\overline{d}(e, \gamma_0^*(\cdot))$
is smooth and $\gamma_0^*(\tau)$ is given by $\gamma_0^*(\tau) = \gamma_b^*(1-\tau)$ with

$$\begin{cases} \dot{\gamma}_b^*(\tau) = -W(q)\,(\mathcal{G}^{-1}_{\gamma_b^*(\tau)}\mathrm{d}W)(\gamma_b^*(\tau)), \quad \tau \in [0,1] \\ \gamma_b^*(0) = q, \end{cases}$$

with $W(q)$ the viscosity solution of

$$\begin{cases} \mathcal{G}_q\left(\mathcal{G}_q^{-1}\mathrm{d}W(q), \mathcal{G}_q^{-1}\mathrm{d}W(q)\right) = 1 \text{ for } q \neq e, \\ W(x,y,\pi) = W(x,y,0), \text{ for all } (x,y) \in \mathbb{R}^2, \\ W(0,0,0) = W(0,0,\pi) = 0. \end{cases}$$

Effects on the Maxwell-set

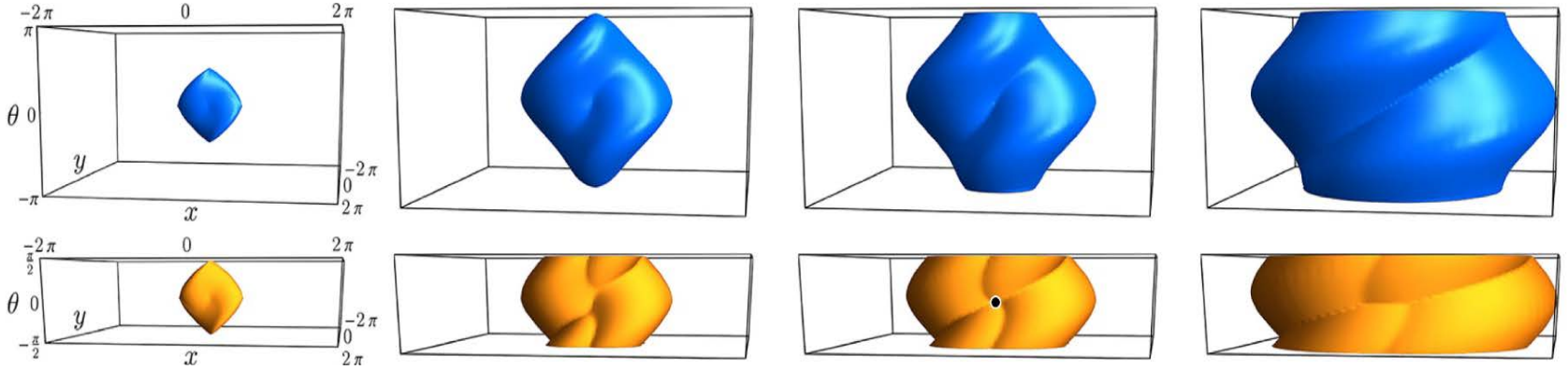

Zoom in in projective line bundle spheres (yellow above):

Sub-Riemannian Spheres on projective line bundle for growing radii:

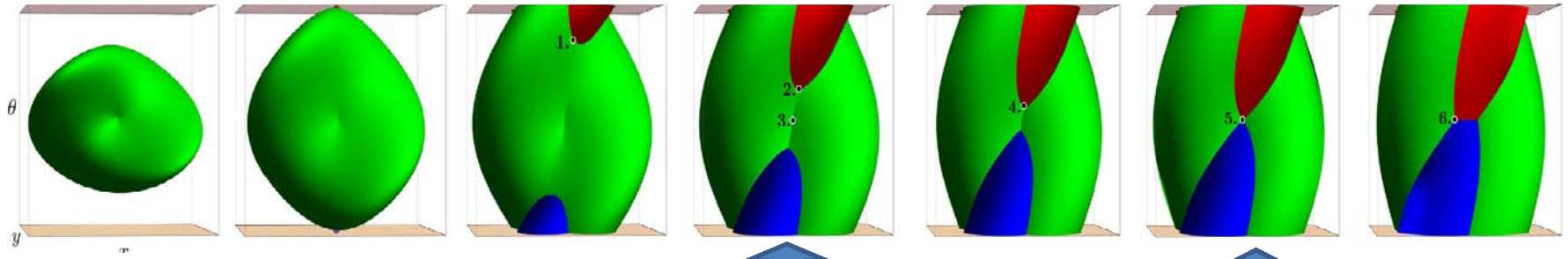

hit conjugate points

hit new 1st Maxwell set $\theta = 0$

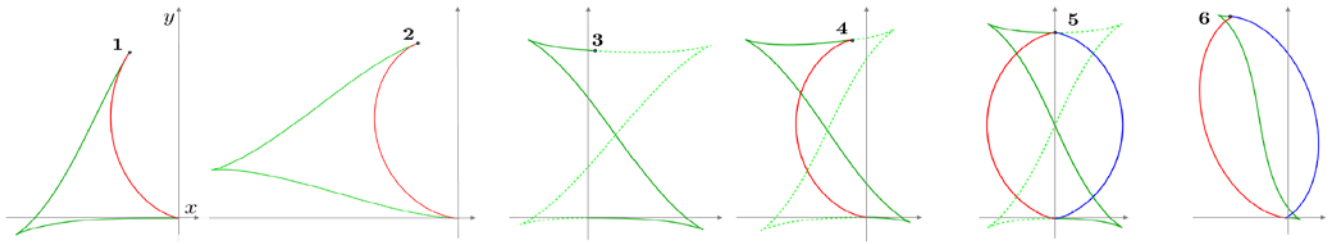

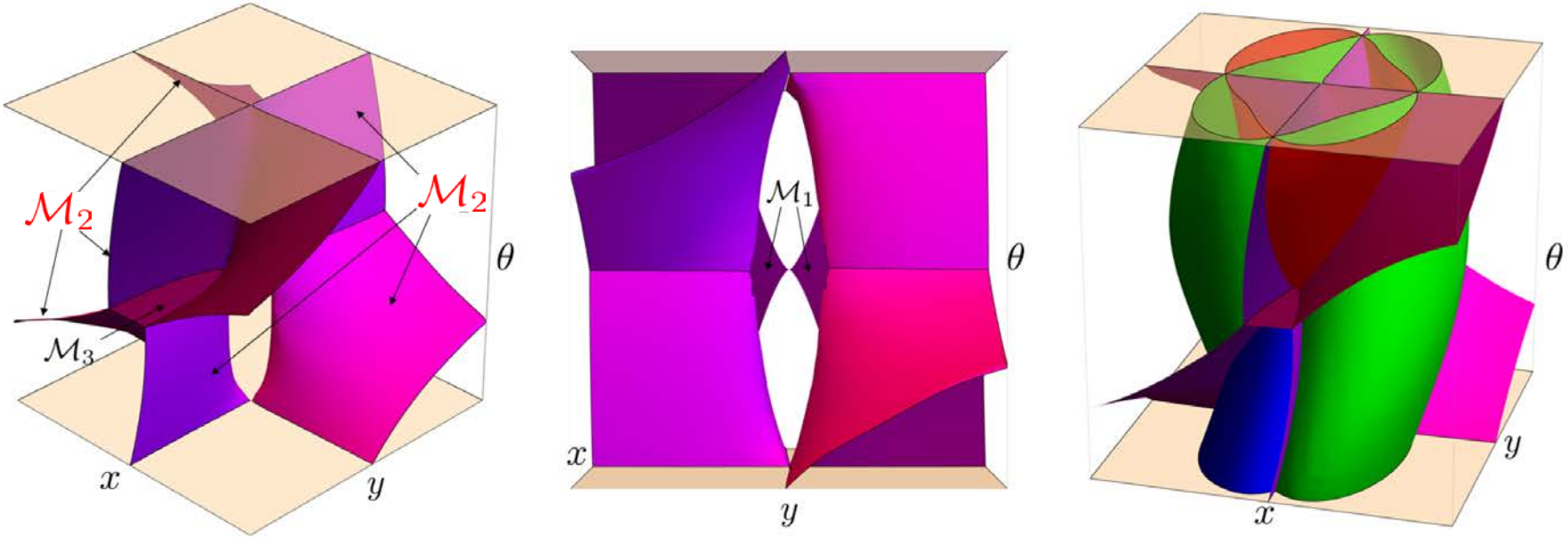

Proposition 2. *Let* $W(q) = \overline{d}(e, q)$ *and let* $W^{\mathrm{SE}(2)}(g) = d(e, g)$. *The Maxwell set* $\mathcal{M}$ *is given by* $\mathcal{M} = \bigcup_{i=1}^{3} \mathcal{M}_i$,

- $\mathcal{M}_1$ *is a part of local component of Maxwell set* $\mathrm{Exp}(\mathrm{MAX}^2)$ *in* $\mathrm{SE}(2)$, *s.t.* $t_1^{\mathrm{MAX}} = W(\gamma(t_1^{\mathrm{MAX}}))$
- New $\mathcal{M}_2$ *is given by* $W^{\mathrm{SE}(2)}(g) = W^{\mathrm{SE}(2)}(g \odot (0, 0, \pi))$
- $\mathcal{M}_3$ *is a part of global component of Maxwell set* $\mathrm{Exp}(\mathrm{MAX}^5)$ *in* $\mathrm{SE}(2)$, *s.t.* $t_1^{\mathrm{MAX}} = W(\gamma(t_1^{\mathrm{MAX}}))$.

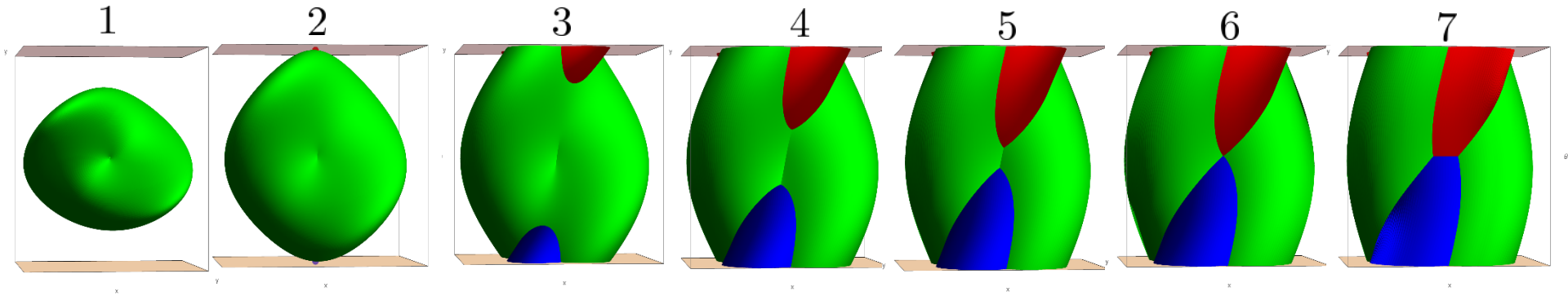

Proposition 3. *The maximal multiplicity ν of a Maxwell point on a SR sphere depends on its radius R. Denote $\mathcal{M}^R = \mathcal{M} \cap \mathcal{S}(R)$ and $\mathcal{M}_i^R = \mathcal{M}_i \cap \mathcal{S}(R)$. One has the following development of Maxwell set*

1. *if $0 < R < \frac{\pi}{2}$ then $\mathcal{S}(R)$ is homeomorphic to S^2 and it coincides with SR sphere in* $\mathrm{SE}(2)$, $\mathcal{M}^R = \mathcal{M}_1^R$ *and* $\nu = 2$;
2. *if $R = \frac{\pi}{2}$ then $\mathcal{S}(R)$ is homeomorphic to S^2 glued at one point, $\mathcal{M}^R = \mathcal{M}_1^R \cup \mathcal{M}_2^R$, $\mathcal{M}_1^R \cap \mathcal{M}_2^R = \emptyset$, and $\nu = 2$;*
3. *if $\frac{\pi}{2} < R < \overline{R}$ then $\mathcal{S}(R)$ is homeomorphic to T^2, $\mathcal{M}^R = \mathcal{M}_1^R \cup \mathcal{M}_2^R$, $\mathcal{M}_1^R \cap \mathcal{M}_2^R = \emptyset$ and $\nu = 2$;*
4. *if $R = \overline{R} \approx \frac{17}{18}\pi$ then $\mathcal{S}(R)$ is homeomorphic to T^2, $\mathcal{M}^R = \mathcal{M}_1^R \cup \mathcal{M}_2^R$, and $\mathcal{M}_1^R$ intersects $\mathcal{M}_2^R$ at four (conjugate) points, $\nu = 2$;*
5. *if $\overline{R} < R < \tilde{R}$ then $\mathcal{S}(R)$ is homeomorphic to T^2, $\mathcal{M}^R = \mathcal{M}_1^R \cup \mathcal{M}_2^R$, and $\mathcal{M}_1^R$ intersects $\mathcal{M}_2^R$ at four points, where $\nu = 3$;*
6. *if $R = \tilde{R} \approx \frac{9}{8}\pi$ then $\mathcal{S}(R)$ is homeomorphic to T^2, $\mathcal{M} = \mathcal{M}_1^R \cup \mathcal{M}_2^R \cup \mathcal{M}_3^R$, $\mathcal{M}_1^R = \mathcal{M}_3^R$, and $\mathcal{M}_2^R$ intersects $\mathcal{M}_1^R$ at two points, where $\nu = 4$;*
7. *if $R > \tilde{R}$ then $\mathcal{S}(R)$ is homeomorphic to T^2, $\mathcal{M}^R = \mathcal{M}_2^R \cup \mathcal{M}_3^R$ and $\mathcal{M}_2^R$ intersects $\mathcal{M}_3^R$ at four points, where $\nu = 3$.*

Serious Reduction of Cusps

Proposition 4. *The set of reachable end-conditions in* $\mathbb{R}^2 \times P^1$ *via 'cuspless' SR geodesics departing from* $e = (0,0,0)$ *is given by*

$$\tilde{\mathfrak{R}} = \{(x,y,\theta) \in \mathrm{PT}(\mathbb{R}^2) \mid (x,y,\theta) \in \mathfrak{R} \text{ or } (x,y,\theta+\pi) \in \mathfrak{R} \text{ or } (-x,y,-\theta) \in \mathfrak{R} \text{ or } (-x,y,-\theta+\pi) \in \mathfrak{R} \text{ or } x = y = 0\}.$$

previously only

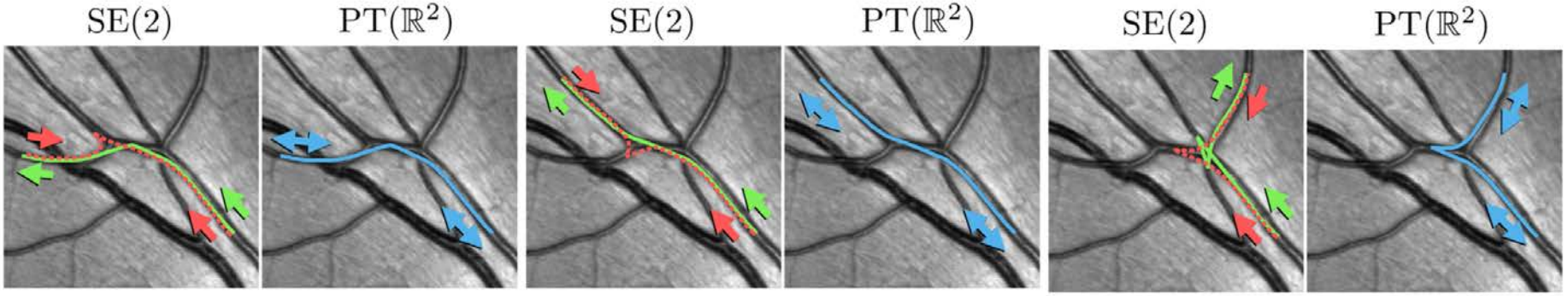

cusps are now rare
but can happen

more examples http://erikbekkers.bitbucket.io/PTR2.html

Conclusion

- Current vessel tracking and enhancement in CAD-tools fail at complex structures, and this can be tackled via orientation scores of 2D/3D images.

- We considered globally optimal path planning in orientation scores where we can deal both with crossings and bifurcations.

- Cusps can be annoying in lifted vessel tracking
  → irreversible Reeds-Shepp car model (JMIV 2017),
  but already much less in projective line bundle (GSI 2017). Prop.4

- The Projective Line bundle structure
  - has great influence on 1st Maxwell set Prop.2 and spheres Prop. 3
  - is easy to implement in Geodesic Tracking Prop.1

Future: Optimal Synthesis ?
& Contour Problem on projective line bundle.